

# Direct Observation of Laser Induced avalanche in a Dielectric.

Stéphane Guizard<sup>1</sup>, Allan Bildé<sup>2</sup>, Sergey Klimentov<sup>3</sup>, Alexandros Mouskeftaras<sup>4</sup>.

*1. Laboratoire Interactions, Dynamiques et Lasers, UMR 9222 CEA, CNRS, Université Paris-Saclay, CEA Saclay, F-91191 Gif-sur-Yvette, France.*

*2. Laboratoire des Solides Irradiés, CEA/CNRS, Université Paris-Saclay, Ecole Polytechnique, 91128 Palaiseau, France,*

*3. General Physics Institute of the Russian Academy of Sciences, Vavilova St 38, 11991 Moscow, Russia.*

*4 Laboratoire LP3, Aix-Marseille University, CNRS, UMR 7341, 13009 Marseille, France.*

## Abstract :

We report the first direct observation of laser induced electronic avalanche in a wide bandgap dielectric, namely silicon dioxide (SiO<sub>2</sub>). A double pulse excitation scheme allows to independently control the plasma density and temperature. Under appropriate conditions, the sequence laser heating-impact ionization can be separated from other photoionization mechanisms, and lead to an obvious increase of the excited carrier density observable by time resolved interferometric measurement of the dielectric function. A model taking into account the non-linear photoexcitation and the dynamics of excited carrier submitted to the heating laser field is used to describe the evolution of the dielectric function and extract quantitative information about the different mechanism efficiency.

The interaction of intense light pulses with transparent materials is a domain of research with a long history which is however more active than ever, and this revival concerns both applied science and fundamental research. It has been shown in the last decade that femtosecond lasers can be used to drill, ablate, cut, or more importantly, to permanently modify – in 3 dimensions - the optical properties of glasses, giving rise to numerous applications in photonics, data storage, microfluidics, etc [1]. As an example, the paper relating the discovery of self-structuring at nanometer scale in the bulk of silica irradiated by femtosecond laser pulses [2] has been cited more than 1000 times. This is because the nano-structuring allows to inscribe and modulate birefringent properties in glasses, hence opening a huge field of application, like 5D data storage [3].

Very recently, another attractive domain has emerged, linked to the possibility to modulate, by using extremely short - few cycles- laser pulses, the optical or insulating properties of dielectric materials [4,5]. Because the period of optical fields is on the order of a femtosecond, the current switching and its control by an optical field may pave a way to petahertz optoelectronic devices [6, 7]. Last but not least, we will mention another active field of research, which is the generation of high order harmonics in transparent solids – for a review see ref [8] while very recently, laser amplification could be observed in an excited Sapphire sample [9].

The shared issue of all this domain is a better knowledge of electronic excitation and relaxation processes in the solid during and immediately after the exciting pulse. It is a challenging task, due to the competition between many different elementary physical mechanism, all occurring at sub-picosecond or femtosecond time scale: electron phonon interaction, elastic and inelastic electron-electron scattering - including impact ionization, formation of transient or permanent defect states, exciton self-trapping, exciton-exciton interaction, etc. The direct observation of these processes is beyond the capacity of traditional time resolved femtosecond experiment due to a lack of temporal resolution.

In this work, we tackle the problem with an alternative technique, using a pump-probe scheme involving a double exciting pulse configuration. An appropriate choice of the characteristics of these two pulses allows to play with the two main parameters of the excited state: plasma density and plasma temperature. The evolution of the solid's dielectric constant is probed during and after the two pulses by time resolved Fourier transform interferometry. The experimental results and numerical simulations support evidence for the first direct observation of laser induced avalanche in a wide band gap dielectric.

The schematic of experimental is drawn on figure 1. The exit of a chirped pulse amplified Ti-Sa laser is split in two parts, which are sent into two separate compressors. One beam, optimally compressed to provide the shortest possible pulses is again split to generate the probe pulse and, after frequency doubling, the first pump pulse. The duration of the second pump pulse, at 800 nm, is expanded for two purposes: reduce the photoexcitation probability, and fit the lifetime of free carrier in SiO<sub>2</sub>, which are known to form self-trapped excitons with a trapping rate of 150 fs [10,11]. The probing part of the setup is built for measuring the variation of the optical constant of the solid during and after the exciting – pump –pulse. The probe beam is going through the sample at varying delay. Then it is split in two parts in a Michelson interferometer, to get two identical probe beams. The two mirrors of this Michelson interferometer are slightly shifted, and their distance to beam splitter is also slightly different. Finally, the image of the entrance surface of the sample is formed with a single lens at the entrance of a spectrometer. This imaging scheme is set such that what is passing through the entrance slit of the monochromator corresponds to an unperturbed part of the beam for the first pulse (reference), and the perturbed part of the beam (which has crossed the excited region of the sample) for the second pulse (signal). These two beams do interfere at the exit of the monochromator. This interference pattern is recorded with a CCD camera and analyzed with a Fourier transform algorithm, allowing to extract the phase shift and the change of fringe

contrast, thus giving access to the modification of the refractive index change induced by the pump pulses.

A first, double pump interferometry measurement is displayed on Figure 2. The time evolution of the phase shift (and absorption) induced by a single pulse at 400 nm (blue curve), at 800 nm (red curve) and when both pulses are applied (black curve). When the sample is excited by the second harmonic only, three parts can be distinguished: first a positive phase shift due to Kerr effect, then a negative phase shift, due to excited carrier, is visible. The population of free carriers decays rapidly, and the signature of the self-trapping process leads to a stable positive phase shift, the third and last part of this curve. The red curve is obtained with the pulse at 800 nm alone. Again, a large positive peak due to Kerr effect is observed. This Kerr signal allows us to check the time position and width of this second pulse. Its intensity is too low to induce a significant excitation density, and no negative phase shift is observed under these conditions. Finally, the black curve is obtained when both pulses are impinging the sample. Similarly, we observe the sequence of positive phase shift, in that case with a double peak due to the two exciting pulses, followed by a short lived negative phase shift which becomes finally positive while excited carriers are self-trapping. The most remarkable feature is an obvious increase of the signal after the Kerr effect when the two pulses are present. The increase is about a factor three for the final positive phase shift, and about a factor 2 for the negative phase shift. The difference between these two factors is essentially due to the Kerr effect which partially overlaps and hides the initial negative phase shift.

We claim that this increase of measured phase shift induced by the sequence of two pump pulses is a first direct observation of an increase of excited carrier density due to laser induced avalanche. Indeed, under our experimental conditions, the only mechanism that can lead to such an increase of the excited carrier density is the following set of events:

- free carriers excitation by the first pulse
- heating of these carrier by the second pulse
- impact ionization: collision between highly excited electrons in the CB and electrons from the top of the valence band, giving two “low energy” carriers in the conduction band. This process can be repeated during the duration of the second pulse, hence the observed increase for the population in the conduction band that we can clearly identify in our double pulse data.
- finally, all excited carriers coming from photoexcitation by the first pulse or from impact ionization, will form self-trapped excitons.

To test this hypothesis, we have increased the delay between the two pump pulses, up to 400 fs. The same set of free temporal pump and double pump scans is reported on Figure 2 (bottom part). The increase of the signal, which can only be seen in the final positive phase shift, is strongly reduced. This behavior is interpreted as follows: with this larger delay between the two pump pulses, a larger fraction of carriers has already been trapped before the second heating pump impinges the sample. These trapped carriers cannot absorb photons from the second pump pulse, and thus do not contribute to the heating-impact ionization - or avalanche - mechanism.

In order to get more quantitative information from these experimental data, we have performed numerical simulations based on the multiple rate equation model first introduced by B. Rethfeld [12]. The various populations are described in the following fashion: the valence band is

described as a single energy level with an electron density  $\rho_{vb}$  and the conduction band, as a series of energy levels of electron density  $\rho_i$  for level  $i$ . The amount of energy separating each of these levels is set to be the one of a photon from the IR pump. Finally, a level is added in the forbidden band to model the population of STE. The set of equations governing the population of the conduction band levels is displayed below:

$$\begin{aligned} \frac{\partial \rho_1}{\partial t} &= \rho_{vb}(\sigma_6 I_{IR}^6 + \sigma_3 I_{UV}^3 + \sigma_{cross} I_{UV}^2 I_{IR}^2) - \left( \sigma_{heat,IR} \frac{I_{IR}}{h\nu_{IR}} + \sigma_{heat,UV} \frac{I_{UV}}{h\nu_{UV}} \right) \rho_1 + 2\tilde{\alpha} \frac{\rho_{vb}}{\rho_{vb,i}} \rho_k \\ &\quad - \frac{\rho_1}{\tau_{ste}} + \rho_{ste} \sigma_{ste} I_{IR}^{n_{ste}} \\ \frac{\partial \rho_2}{\partial t} &= \sigma_{heat,IR} \frac{I_{IR}}{h\nu_{IR}} (\rho_1 - \rho_2) - \sigma_{heat,UV} \frac{I_{UV}}{h\nu_{UV}} \rho_2 - \frac{\rho_2}{\tau_{ste}} \\ &\quad \cdot \\ &\quad \cdot \\ &\quad \cdot \\ \frac{\partial \rho_i}{\partial t} &= \sigma_{heat,IR} \frac{I_{IR}}{h\nu_{IR}} (\rho_{i-1} - \rho_i) - \sigma_{heat,UV} \frac{I_{UV}}{h\nu_{UV}} (\rho_{i-2} - \rho_i) - \frac{\rho_i}{\tau_{ste}} \\ &\quad \cdot \\ &\quad \cdot \\ &\quad \cdot \\ \frac{\partial \rho_k}{\partial t} &= \sigma_{heat,IR} \frac{I_{IR}}{h\nu_{IR}} \rho_{k-1} - \sigma_{heat,UV} \frac{I_{UV}}{h\nu_{UV}} (\rho_{k-2} + \rho_{k-1}) - \tilde{\alpha} \frac{\rho_{vb}}{\rho_{vb,i}} \rho_k - \frac{\rho_k}{\tau_{ste}} \end{aligned}$$

In the first equation, one can see that several excitation and relaxation mechanisms are taken into account. From left to right, multiphoton ionization from the IR pulse and the UV pulse involving the absorption of respectively 6 and 3 photons. Cross excitation involving two UV photons and two IR photons is present, as well as heating of CB electrons by both pulses and impact ionization. Finally, CB electrons can relax as STE and be reexcited through multiphoton ionization in the conduction band. Population of STE and valence band electrons are then modeled by:

$$\begin{aligned} \frac{\partial \rho_{ste}}{\partial t} &= \frac{\rho_{cb}}{\tau_{ste}} - \rho_{ste} \sigma_{ste} I_{IR}^{n_{ste}} \\ \frac{\partial \rho_{vb}}{\partial t} &= - \left( \frac{\partial \rho_{ste}}{\partial t} + \frac{\partial \rho_{cb}}{\partial t} \right) \end{aligned}$$

Where  $\rho_{cb} = \sum_{i=1}^k \rho_i$  is the total electron density in the conduction band. It should be noted that all cross sections are kept constant. In parallel, the evolution of the dielectric constant is calculated using a Drude-Lorentz model:

$$n^2 - 1 = \frac{e^2 f_{vb}}{\epsilon_0 m_{vb}^*} \frac{\rho_{vb}}{\omega_{vb}^2 - \omega^2 - \frac{i\omega}{\tau_{vb}}} - \frac{e^2 f_{cb}}{\epsilon_0 m_{cb}^*} \frac{\rho_{cb}}{\omega^2 + \frac{i\omega}{\tau_{coll}}} + \frac{e^2 f_{ste}}{\epsilon_0 m_{ste}^*} \frac{\rho_{ste}}{\omega_{ste}^2 - \omega^2 - \frac{i\omega}{\tau_{ste}}} + n_{2,IR} I_{IR} + n_{2,UV} I_{UV}$$

Where, in addition to the contribution of all three different populations, Kerr effect has been included. This allows us to calculate the phase shift undergone by the probe pulse when going through the excited medium as well as the changes of reflectivity of the sample's surface. We keep track of the pump pulses intensities by taking into account these changes and through energy conservation. All the values of the parameters used in this model are listed in Table 1 and 2. The calculated results are shown in full lines in figure 2. As one can see, the simulation reproduces the experimental results pretty well. To test the importance of impact ionization in these experiments, we can then define a multiplication factor as follows:

$$m = \frac{\rho_{tot}}{\rho_{tot} - \rho_{ii}}$$

Where  $\rho_{tot}$  is the total excited electron density and  $\rho_{ii}$ , the excited electron density originated from impact ionization. This multiplication factor has been calculated using the model that we just described as a function of space in the sample. These results are shown in figure 3. This figure displays a much more complex geometry that could be anticipated from the experiment alone. Another feature, is the high values of  $m$  reached close to the surface and at the center of the pulses. Indeed, multiplication factors as high as 9 and 8 are reached respectively in the first and second experiments. Such value corresponds to what can be called an electronic avalanche. But what is remarkable is that this avalanche takes place in highly localized regions that depends on the IR pump intensity.

Since the free carrier lifetime is limited in SiO<sub>2</sub>, a more detailed study of the electron multiplication process is needed to clarify the role of double pump excitation, trapping, and reheating. And eventually, clearly separate the respective role of crossed excitation, and reexcitation of carrier by the second pulse before conduction band electrons are trapped.

This is done by using a continuous scanning of the delay between the two pump pulses. For this experiment, the delay between the “blue pump” and the probe pulse is kept constant, while the delay between the two pump pulses is continuously scanned. Since a precise knowledge of the zero delay between the two pump pulses is mandatory, we record the time correlation of the two pulses. As shown in figure 1, we use a non-linear crystal that allows us to produce the sum frequency of the two pump pulses, sitting at the place of the sample. This signal is then isolated using a prism and recorded by a CCD. The result is the inter-correlation function between the two pump pulses, shown by the green dots in figure 4.

The result of this double pump scan is shown in the figure 4 for three different energies of the IR pump. At negative delay, the IR pulse which does not excite carriers, is arriving first. Only a positive signal due to the UV pump is observed. Then, during the overlap of the two pump pulses, around delay 0, we observe a rise of this signal; This is due to the positive phase shift induced by trapped carriers which have been excited by the crossed absorption of IR and UV photons. The signal is positive because these carriers are trapped when the phase shift is measured (remember the probe pulse is arriving 2.5ps later).

Then the most important result is that this increase of positive signal has an asymmetric shape, which lasts longer than the correlation function of the two pump pulses. This is the direct signature of the increase of excited carrier density induced by impact ionization. Indeed, if the IR pulse did not play any role after the UV pulse has passed through the sample (i.e. if there was no impact ionization), the positive phase shift would follow the signal from the intercorrelation function. At higher delays, (1ps to 1.75ps), an intermediate regime is reached where, when the IR pulse comes through the sample, all previously excited electrons have relaxed as STEs. If the IR fluence is high enough, these STEs can be reexcited. This can be seen in figure 4.b) and c) where a negative phase shift is recorded at approximately 2.2ps pump-pump delay. This negative phase shift is indeed the signature of conduction band electrons. At a 2.5ps delay, a peak appears in all three graphs which is attributed to Kerr effect, since the IR pump overlaps with the probe pulse.

In order to quantitatively discriminate the contribution of the various processes taking place in the solid, we applied the same model as previously to this experiment. The agreement between the simulation results (in orange full line in Figure 4) and the experimental results is quite satisfactory. The calculated contributions to the excited electron density of impact, multiphoton and crossed ionizations are shown in figure 5 as a function of pump-pump delay. As can be seen, there is a temporal window corresponding to a pump-pump delay of 200-500fs where the impact ionization largely dominates the interaction. This temporal window corresponds to the moment where electrons have been excited by the UV pump and are not yet trapped as STEs. Another feature of interest is the evolution of the relative importance of impact and multiphoton ionizations at long pump-pump delays. As the IR pump intensity increases, impact ionization becomes dominant. This is due to the growing importance of de-trapping. In this regime, the IR pump goes through the sample much later (>1.5ps later) than the UV pump, so every previously excited carriers have relaxed as STEs. If the IR pump is intense enough, these STEs can be re-excited, and created conduction band electrons can then be heated and generate impact ionization.

To summarize, an original scheme involving two colors pumps has been implemented to produce a direct proof of the existence of impact ionization in crystalline SiO<sub>2</sub>. First, a set of experimental conditions has been chosen to provide a quantitative proof of principle. Then the experimental has been modified and the role of several experimental parameters has been studied. A model based on multiple rate equations that quantitatively reproduces the experimental data has also been implemented. It has been found that the relative importance of

impact ionization displays a complex geometry inside the sample, and that under certain conditions avalanche can take place in some regions of it. Obviously the region at the surface and just beneath is where the most important multiplication effect can be observed. Time resolved reflectivity change [13] should be an appropriate tool to probe the dramatic plasma density evolution at the surface. An optimal temporal window for pump-pump delay have also been detected to maximize the effect of impact ionization. It should be noted we have carried out the same kind of experiment in other materials, namely  $Al_2O_3$  and  $MgO$ , where no avalanche effect could be observed at all, despite extreme intensity conditions, very far above optical breakdown threshold, have been explored. Therefore it seems that exciton self-trapping and electronic avalanche or impact ionization appear to be altogether competitive *and* cooperative mechanisms. Further experiment on other materials where the formation of self-trapped excitons, like for instance alkali halides, should be carried out to further investigate a link between exciton self-trapping and impact ionization in wide band gap materials.

## References :

- [1] R. R. Gattas and E. Mazur, *Nature Photonics* 2, 219-225 (2008).
- [2] Y. Shimotsuma, *et al.* *Phys. Rev. Lett.* 91, 247705 (2003)
- [3] J. Zhang, M. Gecevičius, M. Beresna, and P. G. Kazansky, *CLEO: 2013 Postdeadline*, OSA Postdeadline Paper Digest (online) (Optical Society of America, 2013),
- [4] A. Schiffrin et al, *Nature* 493, p.70, 2013.
- [5] M. Schultze et al, *Nature* 493, p.75, 2013.
- [6] Kwon, O. et al., *Sci. Rep.* 6,21272; doi: 10.1038/srep21272.
- [7] Hiroki Mashiko, Katsuya Oguri, Tomohiko Yamaguchi, Akira Suda and Hideki Gotoh, *Nature physics*, 12, 741, 2016.
- [8] S. Ghimire et al. *J. Phys. B: At. Mol. Opt. Phys.* 47 (2014) 204030
- [9] Thomas Winkler, Lasse Haahr-Lillevang, Cristian Sarpe, Bastian Zielinski, Nadine Götte, Arne Senftleben, Peter Balling and Thomas Baumert, *Nature Physics*, 2017;
- [10] K. Tanimura, T. Tanaka, and N. Itoh, *Phys. Rev. Lett.* 51, 423 (1983).
- [11] Audebert P., Daguzan Ph., Dos Santos A., Geindre J.P., Guizard S., Hamoniaux G., Krastev K., Martin Ph., Petite G., Antonetti A., *Phys. Rev. Lett.* ,52, 1994.
- [12] B. Rethfeld, *Phys. Rev. B.* 73, 035101, 2006.
- [13] M. Garcia-Lechuga, L. Haahr-Lillevang, J. Siegel, P. Balling, S. Guizard, and J. Solis, *Phys. Rev. B* 95, 214114 (2017).

Figures captions:

- Figure 1: schematic drawing of the double pump-interferometric probe setup.  $f_1$ ,  $f_2$  and  $f_3$  are pre-focusing, focusing and imaging lens, respectively.

- Figure 2: time resolved interferometry signal with UV alone (blue), IR alone (red), and both pump pulses (black). The dots represent the experimental measurements and full line, the results of simulation. The incident fluences are for the UV pump: a), b)  $1,32 J/cm^2$ , c), d)  $0,70 J/cm^2$  and for the IR pump: a), b)  $1,43 J/cm^2$ , c)  $0,94 J/cm^2$  d)  $1,66 J/cm^2$ . The delay between the two pulses is a) 200 fs and b), c), d) 380 fs.

- Figure 3: excited electrons multiplication factor due to impact ionization calculated via the MRE model as a function of radial coordinate and depth in the sample. Irradiation conditions corresponds to that of the figure 2.

- Figure 4: time resolved interferometry signal using both pump pulses (black dots) as a function of pump-pump delay. Results given by the simulation is displayed in orange full line. Green dots represent the measured third harmonic signal. UV pump fluence is  $1,12 J/cm^2$ , and IR pump fluence is a)  $1,30 J/cm^2$ , b)  $2,13 J/cm^2$ , and c)  $3,13 J/cm^2$ . Figures d), e) and f) are respectively zooms from figures a), b) and c).

- Figure 5: Average relative contributions to the excited electron density of impact ionization, multiphoton ionization and crossed multiphoton ionization as a function of pump-pump delay. The average has been made over a cylindric volume of radius the HWHM of the UV pump pulse and depth  $100\mu m$ . Irradiation conditions of figures a), b) and c) are respectively the same as in figure 4. a), b) and c).

Tables captions:

Table 1: Material parameter values used in the numerical simulation

Table 2: Laser-matter interaction parameter values used in the numerical simulation

Figure 1 :

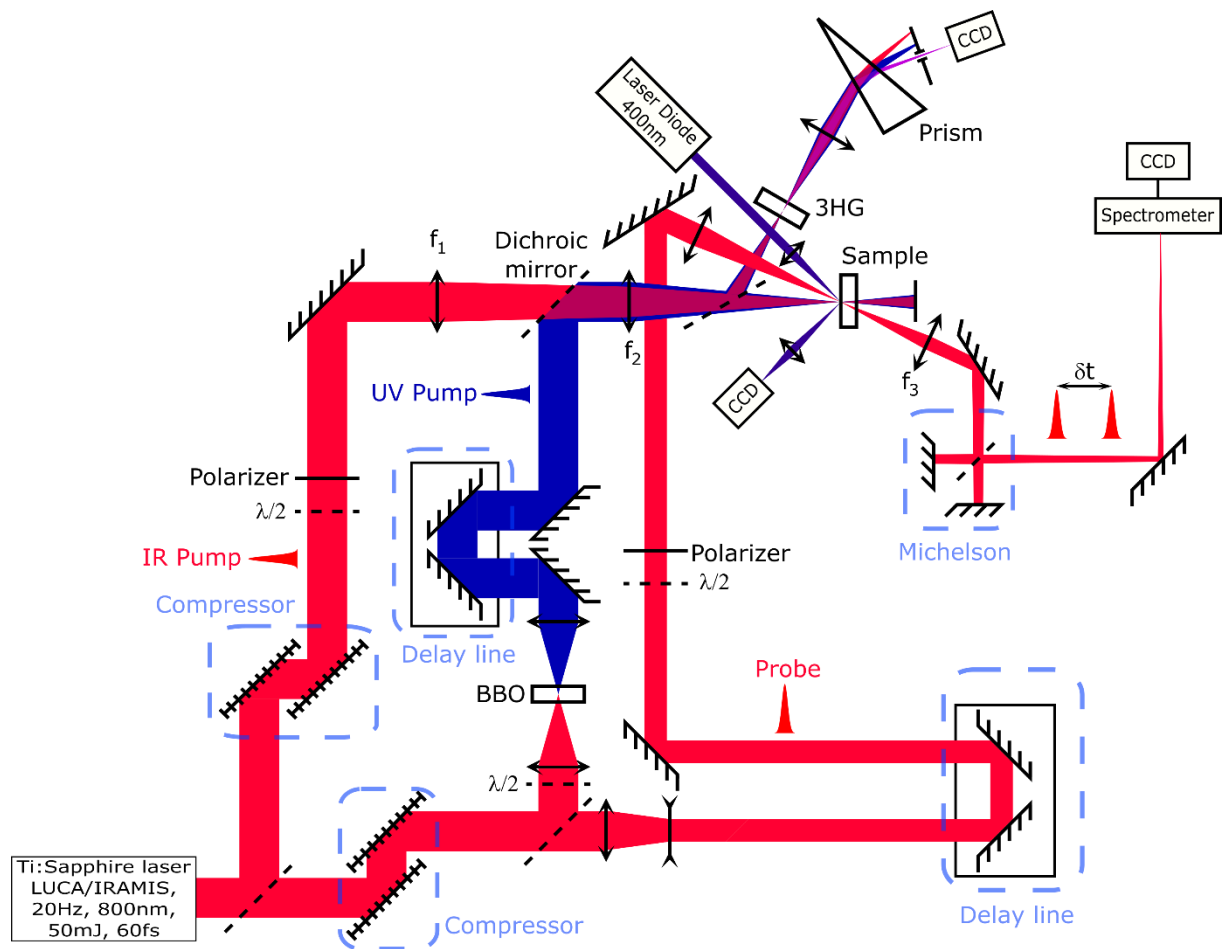


Figure 2:

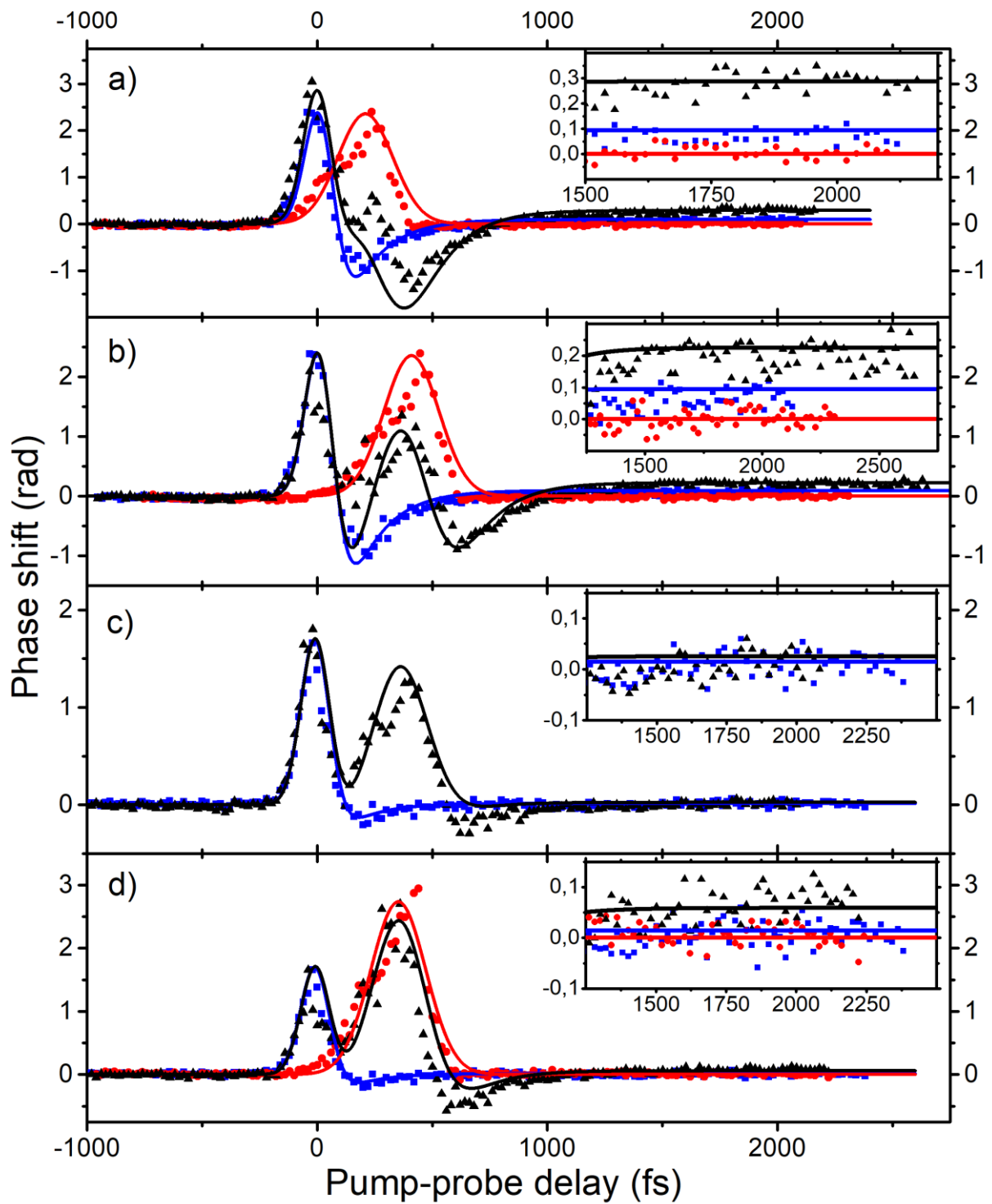


Figure 3 :

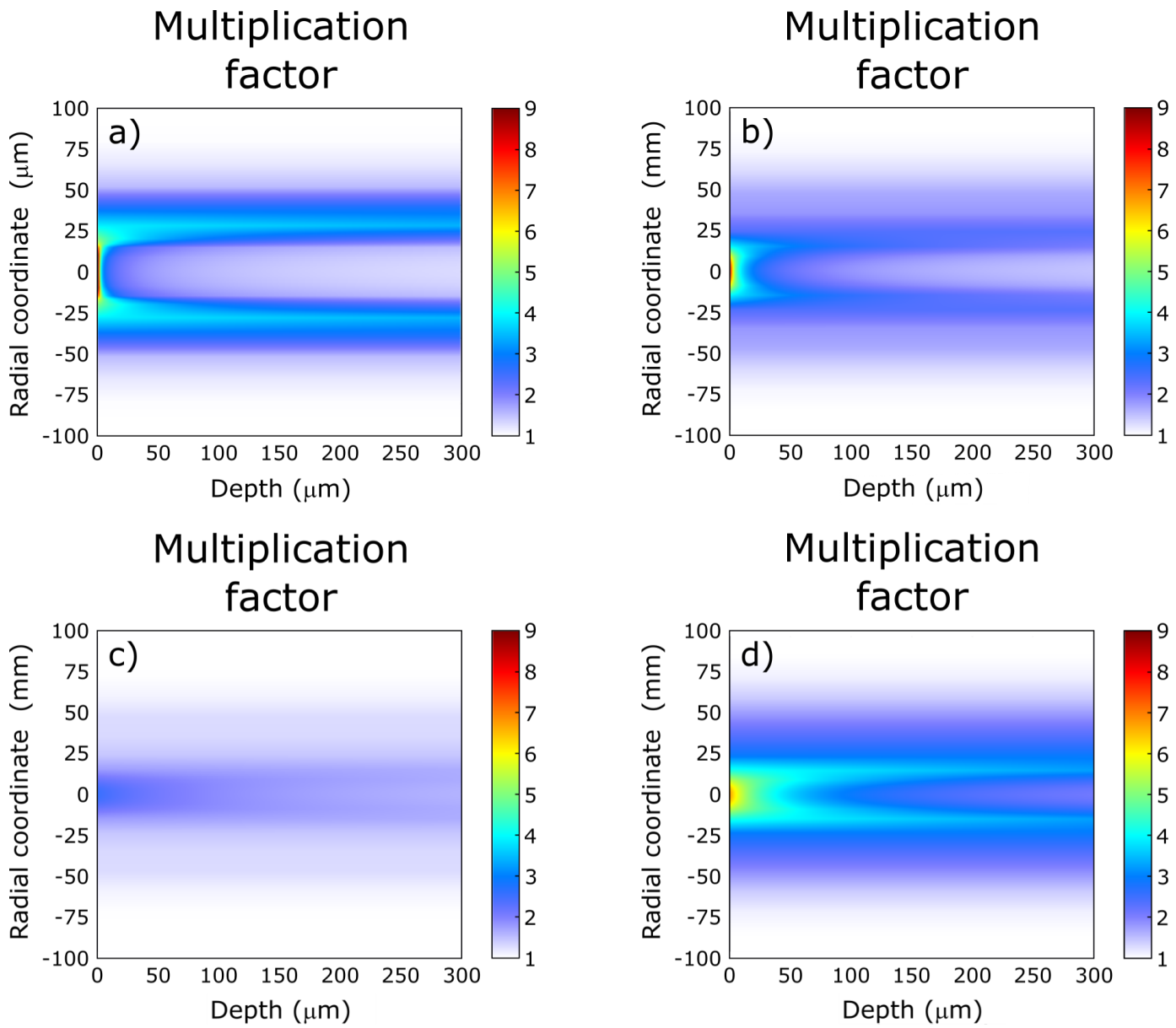


Figure 4 :

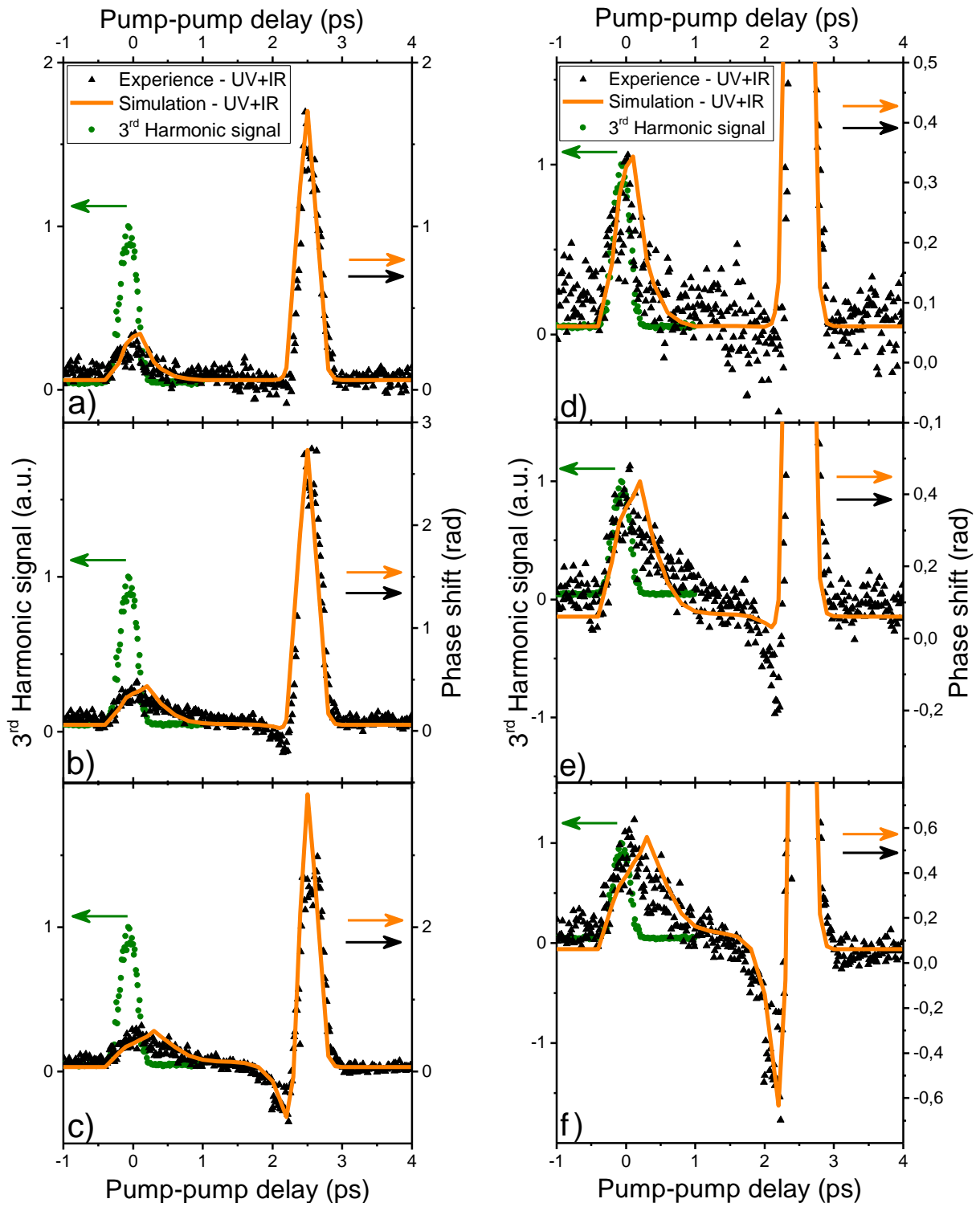


Figure 5 :

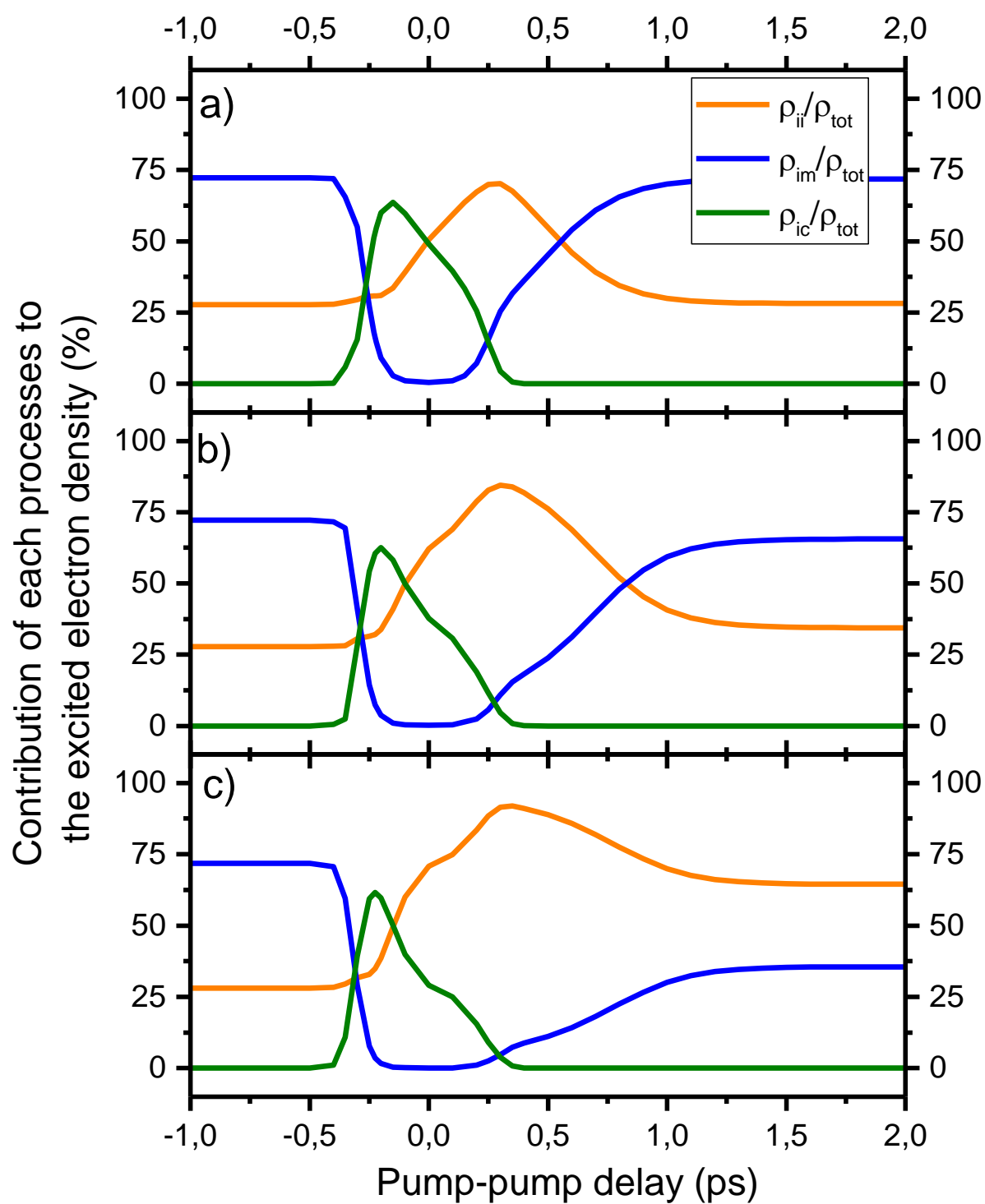


Table 1 :

$E_{gap}$ (ev)	9
$\rho_{v,i}$ ( $cm^{-3}$ )	$2.2 \cdot 10^{22}$
$\tilde{\alpha}$ ( $s^{-1}$ )	$1.0 \cdot 10^{14}$
$m^*/M_e$	0.64
$f_{vb}$	2.88
$f_{cb}$	1.00
$f_{ste}$	1.30
$\tau_{coll}$ (fs)	0.75
$\tau_{ste}$ (fs)	150
$\tau_{vb}$ (fs)	800
$\hbar\omega_{ste}$ (ev)	5.2

Table 2 :

	400nm pump	800nm pump
$n$	3	6
$\sigma_n$ ( $m^{2n} \cdot s^{-1} \cdot W^{-n}$ )	$2.45 \cdot 10^{-41}$	$4.70 \cdot 10^{-97}$
$n_{ste}$	/	4
$\sigma_{ste}$ ( $m^{2n_{ste}} \cdot s^{-1} \cdot W^{-n_{ste}}$ )	/	$5.30 \cdot 10^{-57}$
$\sigma_{cross}$ ( $m^8 \cdot s^{-1} \cdot W^{-4}$ )	$1.0 \cdot 10^{-55}$	$1.0 \cdot 10^{-55}$
$\sigma_{heat}$ ( $m^2$ )	$7.5 \cdot 10^{-22}$	$1.1 \cdot 10^{-21}$
$n_2$ ( $cm^2 \cdot W^{-1}$ )	$2.4 \cdot 10^{-16}$	$2.9 \cdot 10^{-16}$